Journal of Applied Physics

Sinusoidal and rectangular Bragg grating filters: Design, fabrication, and comparative analysis

Cite as: J. Appl. Phys. **132**, 064501 (2022); https://doi.org/10.1063/5.0098923
Submitted: 13 May 2022 • Accepted: 14 July 2022 • Published Online: 08 August 2022

Hamed Saghaei, Payam Elyasi and Bhavin J. Shastri

Journal of Applied Physics ARTICLE scitation.org/journal/jap

Sinusoidal and rectangular Bragg grating filters: Design, fabrication, and comparative analysis

Cite as: J. Appl. Phys. **132**, 064501 (2022); doi: 10.1063/5.0098923
Submitted: 13 May 2022 · Accepted: 14 July 2022 ·
Published Online: 8 August 2022

Hamed Saghaei,[1,2,a] Payam Elyasi,[1,2,b] and Bhavin J. Shastri[3,c]

AFFILIATIONS

[1]Department of Electrical Engineering, Shahrekord Branch, Islamic Azad University, Shahrekord, Iran
[2]Energy Research Center, Shahrekord Branch, Islamic Azad University, Shahrekord, Iran
[3]Department of Physics, Engineering Physics, and Astronomy, Queen's University, Kingston, Ontario K7L 3N6, Canada

[a]**Author to whom correspondence should be addressed:** h.saghaei@iaushk.ac.ir
[b]payam.elyasi@gmail.com
[c]shastri@ieee.org

ABSTRACT

In this paper, we compare the characteristics of several waveguide Bragg gratings (WBGs) with sinusoidal and rectangular corrugated sidewalls in high confinement integrated optics. Our measurements confirm the performance of both the rectangular and sinusoidal grating as band-rejection filters for TE-polarized signals in the telecom C-band. These measurements demonstrate record high extinction ratios of 35 and 28.91 dB for sinusoidal and rectangular WBGs with a rejection bandwidth as narrow as 4.42 and 6.165 nm. The simulation results and measurements show that the filter bandwidth and coupling coefficient can be changed by altering the corrugation width (ΔW), allowing us to control the filter's quality factor precisely. The bandwidth of rectangular WBGs drops for $\Delta W > 80$ nm, constraining the design of devices requiring broadband WBGs. In contrast, the bandwidth of sinusoidal WBG continues to increase for $\Delta W > 80$ nm, providing a wider bandwidth for designers. These findings demonstrate the potential for effective integration of new photonic functionalities into low-footprint electro-optical waveguide tools for sensing, communicating, and computing applications.

I. INTRODUCTION

Waveguide Bragg grating (WBG) based on a silicon-on-insulator platform has various applications in the fabrication of photonic integrated circuits (PICs) due to its unique features, especially as a coupler. These structures were first proposed by Murphy *et al.*[1] in 2001. There are different optical grating-based waveguides and fibers, but generally grating with physical corrugation in silicon waveguides has filter and coupler applications.[2] This contrasts with Bragg grating optical fibers composed of silica, which are fabricated by applying high-intensity ultraviolet rays to change the refractive index of the core periodically. In WBGs, grating corrugations are on the sidewalls or on the top surface,[3–6] in which the sidewalls are corrugated either on the rib[2,7–9] or on the slab.[10,11] Typically, the top-surface-corrugated configuration possesses a fixed etch depth. Thus, the grating coupling coefficient has a fixed value. Over the past decade, different tools and grating structures have been fabricated, including uniform and sampled gratings,[12] apodized gratings,[13,14] high-Q phase-shifted grating cavities,[15] and grating-assisted contra-directional couplers.[16,17] In sidewall corrugated WBGs, we can easily control the corrugation width. This is essential for complex grating profiles, including apodized gratings to suppress reflection sidelobes.[5] WBGs are used explicitly as notch filters and optical add-drop multiplexers. However, despite considerable progress, there are still numerous challenges. The performances of silicon WBGs depend on the fabrication process since they are typically based on small physical corrugations and can be affected simply by fabrication imperfections like optical lithography smoothing effect,[18] silicon thickness variations,[19] and quantization errors owing to the finite mask grid size. Typically, WBGs possess relatively large grating coupling coefficients, indicating their relative shortness with large bandwidths. Nevertheless, long grating lengths and small coupling coefficients are essential to obtain thinner bandwidths and larger extinction ratios (ERs).[20,21]

Numerous methods exist to obtain small coupling coefficients for WBGs, for example, by utilizing small sidewall corrugations on the strip waveguide (< 10 nm).[12] The limitations of fabrication lithography make the manufacturing of these small corrugations challenging. To utilize rib waveguides with larger corrugations on the slab or the rib sidewalls of the waveguide is another method. Nevertheless, two etch stages are required,[8] increasing the fabrication cost. Typically, strip waveguides possess submicrometer cross-sections (such as 500 nm wide and 220 nm thick[12]), and light is strongly confined in the core area, owing to the high refractive index contrast between the cladding and the core. The rectangular grating corrugations are usually on the waveguide sidewalls; thus, a single lithography step can determine the waveguide and grating.[12] The maximum extinction ratio (ER) of such waveguides is limited by robust polarization scattering,[22] preventing their utilization in applications that require a high ER, such as quantum circuits.[23–25] The Mach–Zehnder interferometer (MZI) is one of the most useful components for photonic integrated circuits.[26] Higher ER filters can be realized with more complex designs, such as Bragg gratings combined with MZIs,[27] coupled-ring resonators,[25] or surface plasmon resonance ring resonator structures.[28] The results of articles reported so far demonstrate that the experimental bandwidth of WBGs is about tens of nanometers.[29] However, the lowest bandwidth reported by Wang *et al.* is about 1 nm.[12] The lithography smoothing effect is one of the challenges during the fabrication and makes small corrugations in the sidewalls difficult. Our studies show that the bandwidth of rectangular WBGs increases from $\Delta W = 20$ nm to $\Delta W = 80$ nm and drops at $\Delta W > 80$ nm. In other words, the bandwidth curve in terms of corrugation width at $\Delta W = 80$ nm has an extremum. Therefore, if the frequency response of the filter is calculated, the corrugation width can have a value in the first interval ($\Delta W > 80$ nm) or the second interval ($\Delta W < 80$ nm), which contradicts the reversibility of the filter behavior. However, using sinusoidal WBGs can overcome this issue.

This paper considers sinusoidal WBGs to achieve a narrower rejection bandwidth, less sensitivity to fabrication imperfection, and an increase in bandwidth at $\Delta W > 80$ nm. Also, this paper evaluates the effect of waveguide widths, grating periods, and waveguide lengths on the transmission spectra of both sinusoidal and rectangular WBGs and compares the results. Our findings show that in the sinusoidal WBG, the bandwidth in terms of ΔW has a relatively increasing trend. We also compare the ER and full width at half maximum ($\Delta\lambda_{FWHM}$(nm)) of these two types of WBGs. These two WBGs could have applications in sensing, communication, and computing.[30–32]

II. MATHEMATICAL BACKGROUND

The fundamental principle behind a WBG is Fresnel equations; when light travels between two media with different refractive indices, it may reflect and/or refract at the interface of two media. The reflected wavelength (λ_β), called the Bragg wavelength, is

$$\lambda_\beta = 2\Lambda n_{eff}, \tag{1}$$

where Λ is the grating period and n_{eff} is the effective refractive index of the grating in the waveguide core that depends on the wavelength and the mode of the light inside the waveguide. The desired reflected wavelength, λ_β, is 1550 nm in this study. For WBGs with rectangular and sinusoidal sidewalls which have a stepwise effective index variation as represented in Fig. 1, the reflection at each interface can be written as $\Delta n/2n_{eff}$, where $\Delta n = n_{eff2} - n_{eff1}$.[11] Each grating period has a role in two reflections; thus, the coupling coefficient is[11]

$$\kappa = \frac{\Delta n}{n_{eff}\Lambda} = \frac{2\Delta n}{\lambda_\beta}. \tag{2}$$

For a sinusoidal grating, effective index variation is

$$n(z) = n_{eff} + 0.5\Delta n.\cos(2\beta_0 z), \tag{3}$$

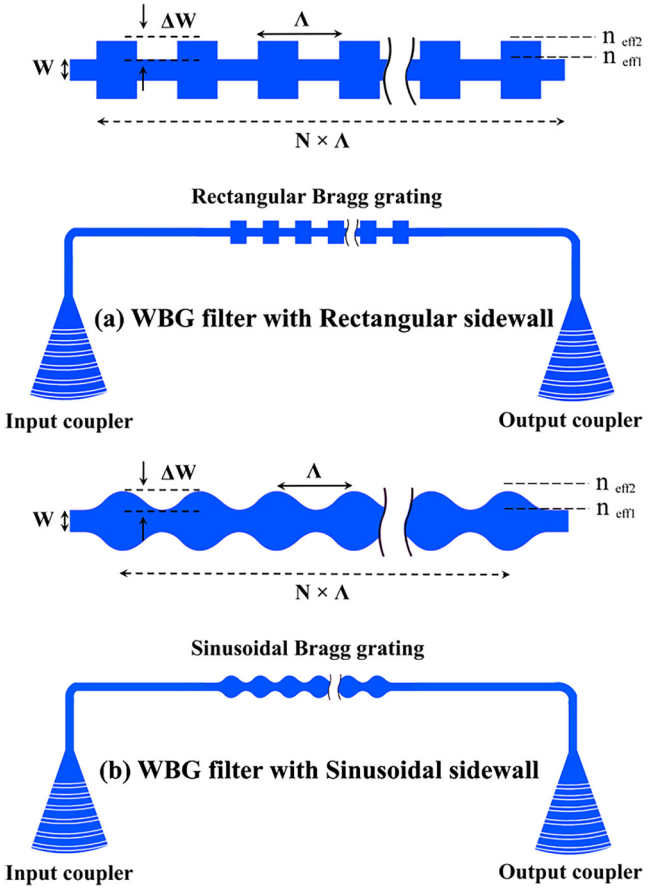

FIG. 1. WBG filters with (a) rectangular and (b) sinusoidal sidewalls. *W* is the waveguide width; ΔW is the corrugation width on each sidewall; *N* is the number of grating periods; Λ is the grating period, and $L = N\Lambda$ is the grating length.

TABLE I. Sellmeier coefficients of Si and SiO_2 used in this paper.

	Sellmeier coefficients					
Materials	B1	C_1 (μm^2)	B2	C_2 (μm^2)	B3	C_3 (μm^2)
Si	9.733	0.0844	0.936	0.134	…	…
SiO_2	0.696	0.0046	0.408	0.0135	0.897	97.93

where β_0 is the Bragg propagation constant[11,33]

$$\beta_0 = \frac{2\pi n_{eff}}{\lambda_\beta}. \tag{4}$$

The coupling coefficient is decreased by a factor of $\pi/4$.[33] For a uniform grating with an L length, the reflection coefficient can be described by[11,33]

$$r = \frac{-i\kappa \sinh(\gamma L)}{\gamma \cosh(\gamma L) + i\Delta\beta \sinh(\gamma L)}, \tag{5}$$

with

$$\gamma^2 = \kappa^2 - \Delta\beta^2, \tag{6}$$

where $\Delta\beta$ represents the propagation constant deviation from the Bragg wavelength

$$\Delta\beta = \beta - \beta_0 = \frac{2\pi n_{eff}(\lambda)}{\lambda} - \frac{2\pi n_{eff}(\lambda_B)}{\lambda_B} \approx \frac{2\pi n_g}{\lambda_B^2}\Delta\lambda \ll \beta_0. \tag{7}$$

Since the wavelength dependence of the effective index is considered, the group index n_g is[11]

$$n_g = n_{eff} - \lambda \frac{dn_{eff}}{d\lambda}. \tag{8}$$

When $\Delta\beta = 0$, Eq. (7) is $r = i \tanh(\kappa L)$. The peak power reflectivity at the Bragg wavelength is

$$R_{peak} = \tanh^2(\kappa L). \tag{9}$$

III. PROPOSED WAVEGUIDE BRAGG GRATING FILTERS

A. Physical structures

A WBG is a distributed Bragg reflector in a short length of the waveguide core that reflects a narrow range of wavelengths and transmits all others. Figure 1 demonstrates the top view of WBGs with (a) rectangular and (b) sinusoidal profiles of the sidewall on the SOI platform. In every waveguide, the strip waveguide is composed of Si surrounded by a SiO_2 layer with a thickness of 2 μm and a width of 20 μm. The Si core has a thickness of 220 nm to entirely confine the fundamental mode inside its region and has a single-mode waveguide. The waveguide width (W) for both

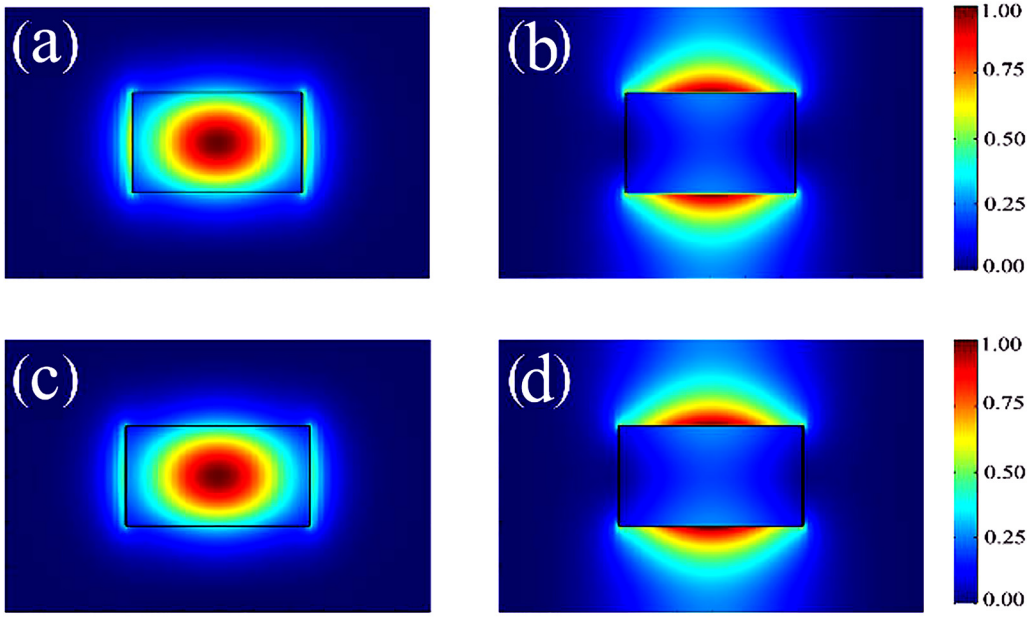

FIG. 2. The electric field distributions of strip waveguide at $\lambda_0 = 1550$ nm for a strip width of 480 nm in (a) TE and (b) TM modes and also for a strip width of 520 nm in (c) TE and (d) TM modes.

waveguides is 500 nm, and the corrugation width (CW; ΔW in Fig. 1) varies from 20 to 120 nm for rectangular and sinusoidal gratings.

An optical fiber is used to couple a laser beam into the waveguide, but the small size of the strip waveguide causes a significant mismatch between them. The core cross-sectional area of the conventional optical fiber (in a 9 μm diameter) is 578 times bigger than the area of the strip waveguide (with dimensions of 500–220 nm). Therefore, we need an optical component to couple the input light accordingly. It is necessary to use an efficient optical device for light coupling from fiber to Si-based PIC and vice versa. A lensed fiber is insufficient to bring the spot size down to that of a waveguide. The Gaussian beam profile for a lensed fiber is much larger than that of the mode of the strip waveguide. Among the various methods that have been proposed to overcome the problem of mode mismatch and coupling photonic integrated circuits, in this paper, we use grating couplers[34] as input and output. Some of the advantages of using grating couplers compared to other methods, such as edge coupling by using Nano tapers on the chip connected to spot size converters or lensed fibers,[35] are lower fabrication costs due to not using post-processing, placement anywhere on the chip, and enabling wafer-level or chip-scale automated testing.

B. Numerical calculations

The eigenmode solver in the Mode solution software is used to calculate the effective refractive index in terms of wavelength by first selecting a cross section of the waveguide. This refractive index depends on the background material's physical properties and the waveguide area. On the other hand, in sinusoidal and rectangular models, the area changes in each waveguide length are calculated and plotted for several regions in terms of wavelength in Fig. 3. The wavelength dependence of the real part of the refractive index for S_i and SiO_2 is modeled by the Sellmeier equation,[36]

$$n^2(\lambda) = A_0 + \sum_{i=1}^{2} B_i \lambda^2 (\lambda^2 - C_i)^{-1}, \tag{10}$$

where constants A_0, B_i, and C_i (μm^2), ($i = 1, 2$), for Si and SiO_2 utilized in this study are listed in Table I.[36] Si having a higher refractive index than SiO_2 over the considered wavelength ranges. Thus, the guiding mechanism in the waveguide core is governed by the total internal reflection (TIR). This large refractive index contrast results in tight light confinement and localization of the optical power inside the core region. Using a full-vectorial modal solver in terms of the finite-difference eigenmode (FDE) expansion method in Lumerical software, we obtained the field distribution of the fundamental mode and propagation constant of the WBG. The method discretizes the waveguide cross section area by a rectangular mesh, and Maxwell's equations are formulated based on a matrix eigenvalue problem. Anisotropic perfectly matched layers (PMLs) are placed on the boundary of the waveguide as absorbing boundaries. For all material interfaces, conformal meshing was also used for reducing meshing errors and increasing the simulations' numerical accuracy.

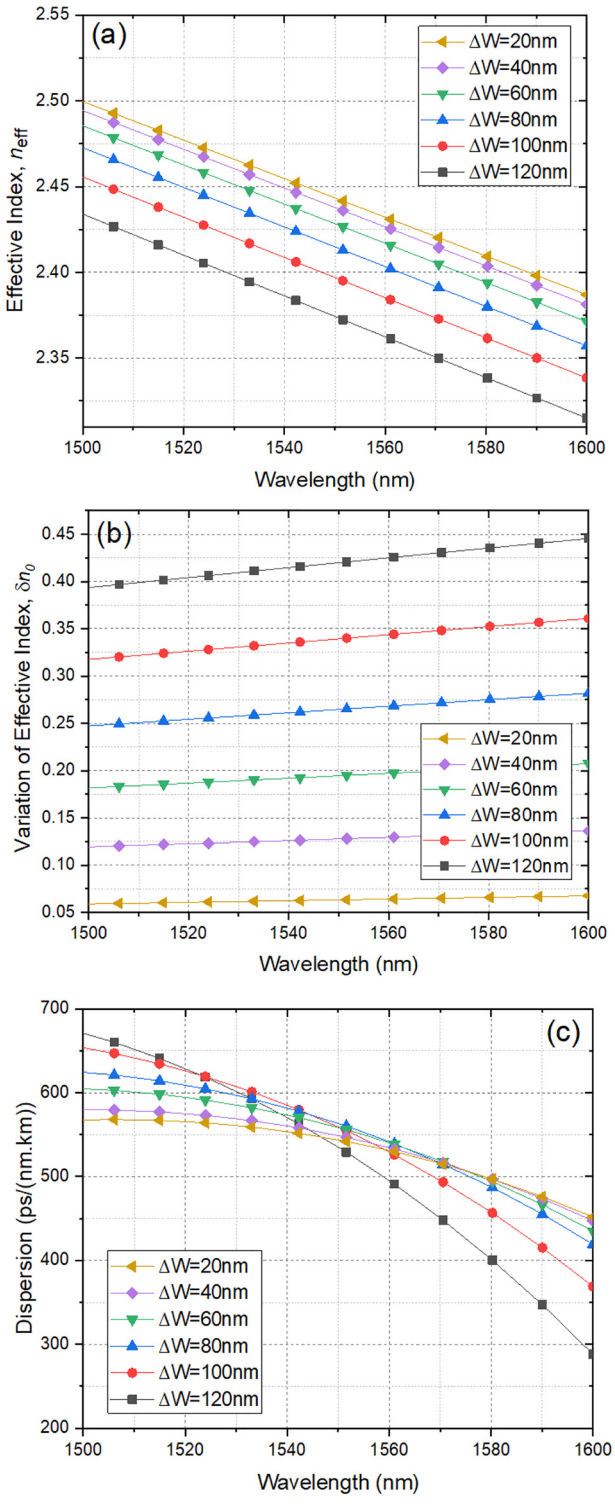

FIG. 3. (a) Effective index, (b) variation of effective index, and (c) dispersion of WBGs for corrugation widths of 20, 40, 60, 80, 100, and 120 nm.

Figure 2 shows the electric field distributions of the proposed strip waveguide at $\lambda_0 = 1550$ nm for a strip width of 480 nm in (a) TE and (b) TM modes and also for a strip width of 520 nm in (c) TE and (d) TM modes. It is observed that the TE mode is mainly confined within the core regions with a slight overlap with the waveguide cladding. Similar field distributions are also gained for the waveguide with different core widths. Also, to obtain a single TE mode at $\lambda_0 = 1550$ nm, we should not only select the waveguide width larger than 310 nm to support a fundamental mode but also select it smaller than 590 nm to avoid higher-order modes.[37] Thus, the strip waveguide with a standard width in TE mode is used in the rest of this paper.

Figure 3 represents the effective index, n_{eff}, and the variation of the effective index,δ_{n0} of WBGs for corrugation widths (ΔW) of 20, 40, 60, 80, 100, and 120 nm. The dispersion of the waveguide observed by the fundamental mode at a wavelength (λ) is determined by[11]

$$D(\lambda) = -\frac{\lambda}{c}\frac{d^2}{d\lambda^2} Re[n_{eff}(\lambda)] = -\frac{2\pi c}{\lambda^2}\beta_2, \tag{11}$$

where c, n_{eff} (λ), and β_2 denote the light velocity in free space, the fiber's effective index, and the second-order dispersion, respectively. Figure 3(c) compares the dispersion profiles of the waveguide in the wavelength range of 1500–1600 nm for different corrugation widths. The plot reveals that increasing the corrugation width increases the negative dispersion slope.

IV. FABRICATION METHOD

Our proposed WBG filters were made by utilizing a 100 keV electron-beam lithography (EBL) procedure. Using an SOI wafer with a 220 nm thick silicon, the fabrication was initiated to make our optical devices on 3 μm thick silicon dioxide as the waveguide cladding. The chip was covered with an electron beam resist rotated at 4000 rpm so that it made a thin layer and afterward soft baked it at 80 °C for 4 min. Then, the chip was placed in an EBL system and exposed to the patterns. The EBL was conducted using a JEOL JBX-6300FS system that acted at an 8 nA beam current, 100 keV energy, and 500 μm exposure field size. The machine grid of 1 nm was utilized for shape placement. The beam stepping grid was 6 nm. An exposure dose of about 2800 C/cm^2 was applied to the structure. The resist was established by immersion in 25% tetramethylammonium hydroxide for 4 min after flowing de-ionized water rinsed for 60 s, isopropanol rinsed for 10 s, and then blown dry with nitrogen. To remove silicon from unexposed areas, inductively coupled plasma etching was used in an Oxford Plasmalab System (OPLS) 100, with a chlorine gas flow of 20 SCCM, a pressure of 12 mT, an ICP power of 800 W, a platen temperature of 20 °C, and a bias power of 40 W, leading to a bias voltage of 185 V. The chips were mounted on a 100 mm silicon carrier wafer during etching through perfluoropolyether vacuum oil. We ensured that everything was fabricated correctly by picturing our WBGs and measuring their dimensions with a scanning electron microscope (SEM). We could also specify the size of the features, such as the width of our waveguides. However, it was challenging, and there was usually 7% inaccuracy in the fabrication process. To deposit 2 μm oxide cladding, plasma-enhanced chemical vapor deposition (PECVD) was used in an Oxford Plasmalab System 100 with silane (SiH_4) flow of 13 SCCM, nitrous oxide (N_2O) flow of 1000 SCCM, high-purity nitrogen (N_2) flow of 500 SCCM, high-frequency RF power of 120 W, the pressure at 1400 mT, and a platen temperature of 350 °C. The oxide covered the entire chip. It was beneficial to protect our devices from dust, scratching, and changes to the surface due to water absorption or oxidation. The final step was to dice the chip. Figure 4 represents the SEM image (top view) of the fabricated WBG filters with (a) rectangular and (b) sinusoidal profiles of the sidewall. To realize the gratings, periodic sidewall corrugations were introduced. Therefore, the gratings and the waveguides can be determined within a one-step lithography technique. Owing to the small optical mode size and waveguide geometry, a small perturbation can cause a

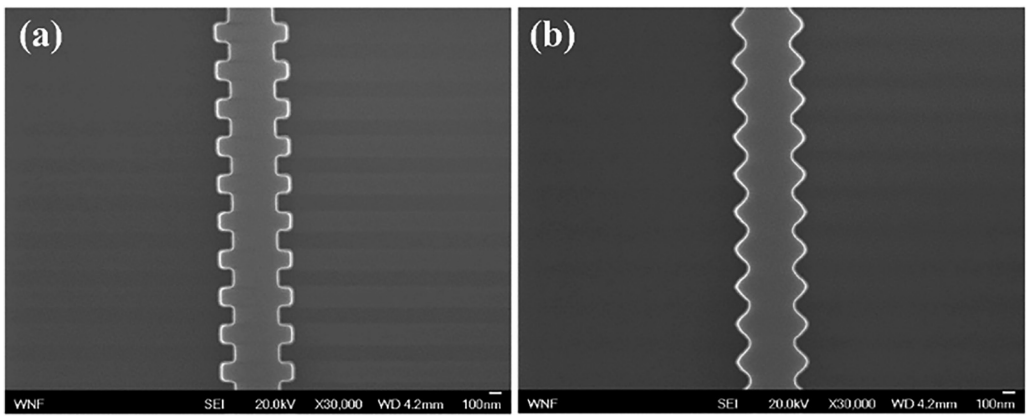

FIG. 4. SEM images of WBGs with (a) rectangular and (b) sinusoidal profiles of the sidewall.

significant grating coupling coefficient on the sidewalls leading to a large bandwidth.

V. RESULTS AND DISCUSSION

To assess the performance of Bragg gratings, several WBG filters with different corrugation widths in the form of rectangular and sinusoidal were designed and fabricated. Figure 5 shows the schematic view of an advanced setup utilizing a multi-channel fiber array to measure the transmission spectra of every WBG. While the fiber array is fixed during the measurement, the chip is put on an automated micro-positioning step. The measurement is fully automated. The software loads a file containing the coordinates of all the GCs. This software passes the stage for aligning a specific set of GCs with the fiber array to record the data, conduct the wavelength sweep, and automatically proceed with the following tool. We use a high-end tunable laser (Agilent 81600B opt. 201) with a wide tuning range (1460–1640 nm), high sweep speeds, and high wavelength accuracy. A dual-channel optical power sensor (Agilent 81635A) simultaneously measures transmission and reflection. Based on this method, the minimum resolution of the spectral measurements is 0.1 pm. Due to the higher refractive index contrast, photonic silicon devices have an increased sensitivity to variations in physical dimensions (e.g., waveguide width and corrugation width) during the lithography process. Although we consider the waveguide width 500 nm in the initial design, variations made during fabrication can reduce the waveguide width. Figure 6 represents the measured transmission spectra of four devices with different waveguide widths but the same corrugation width. Since the interaction between the sidewall corrugation and the optical mode becomes stronger on the narrower waveguide,[38] it is observed that the bandwidth is larger on the narrower waveguide for both sinusoidal and rectangular WBGs. As discussed in Sec. III, Bragg wavelength, λ_β, is directly proportional to the grating period, Λ. This allows us to control the wavelength of the filter by changing the grating period. Figure 7 demonstrates the measured transmission spectra of fabricated WBGs with the rectangular and sinusoidal sidewall of $\Delta W = 100$ nm for (a) $\Lambda = 321.5$ nm, (b) $\Lambda = 325$ nm, and (c) $\Lambda = 331.5$ nm. Bragg wavelength shifts toward longer wavelengths for WBG with

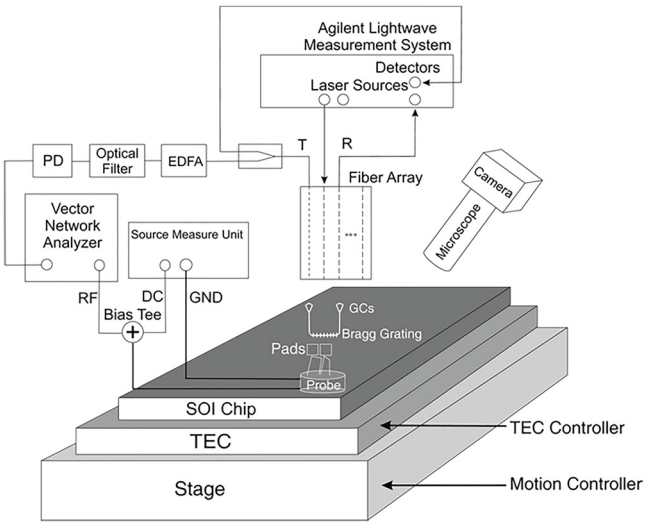

FIG. 5. The schematic view of the advanced experimental setup to measure the spectral response of each WBG shown in Fig. 1 with different corrugation widths. PD: photodetector; EDFA: erbium-doped fiber amplifier; TEC: thermo-electric cooler.

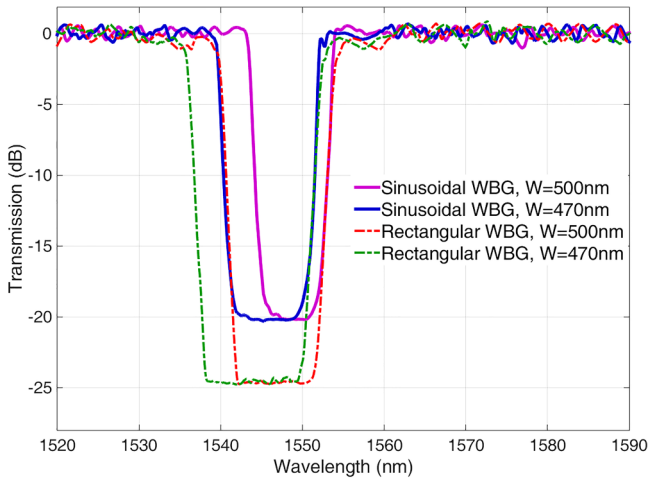

FIG. 6. Measured transmission spectra for sinusoidal and rectangular WBGs with 40 nm corrugation on a 500 nm waveguide and a 470 nm waveguide. Fixed parameters: air cladding, $\Delta W = 40$ nm. and $N = 1000$.

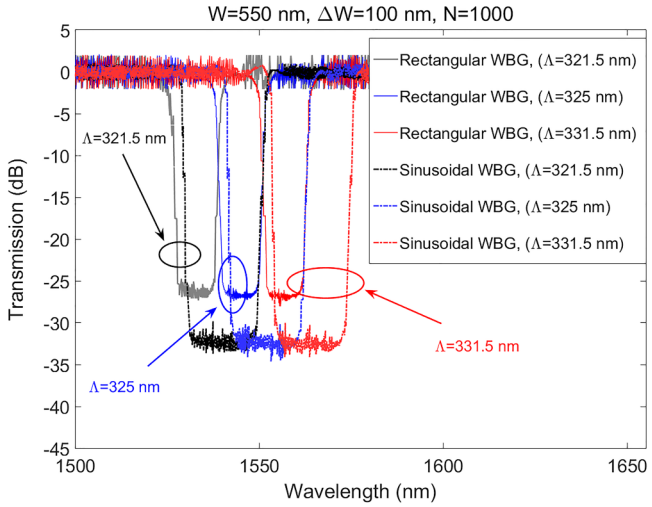

FIG. 7. The measured transmission spectra of fabricated WBGs with the rectangular and sinusoidal sidewall of $\Delta W = 100$ nm for (a) $\Lambda = 321.5$ nm, (b) $\Lambda = 325$ nm, and (c) $\Lambda = 331.5$ nm.

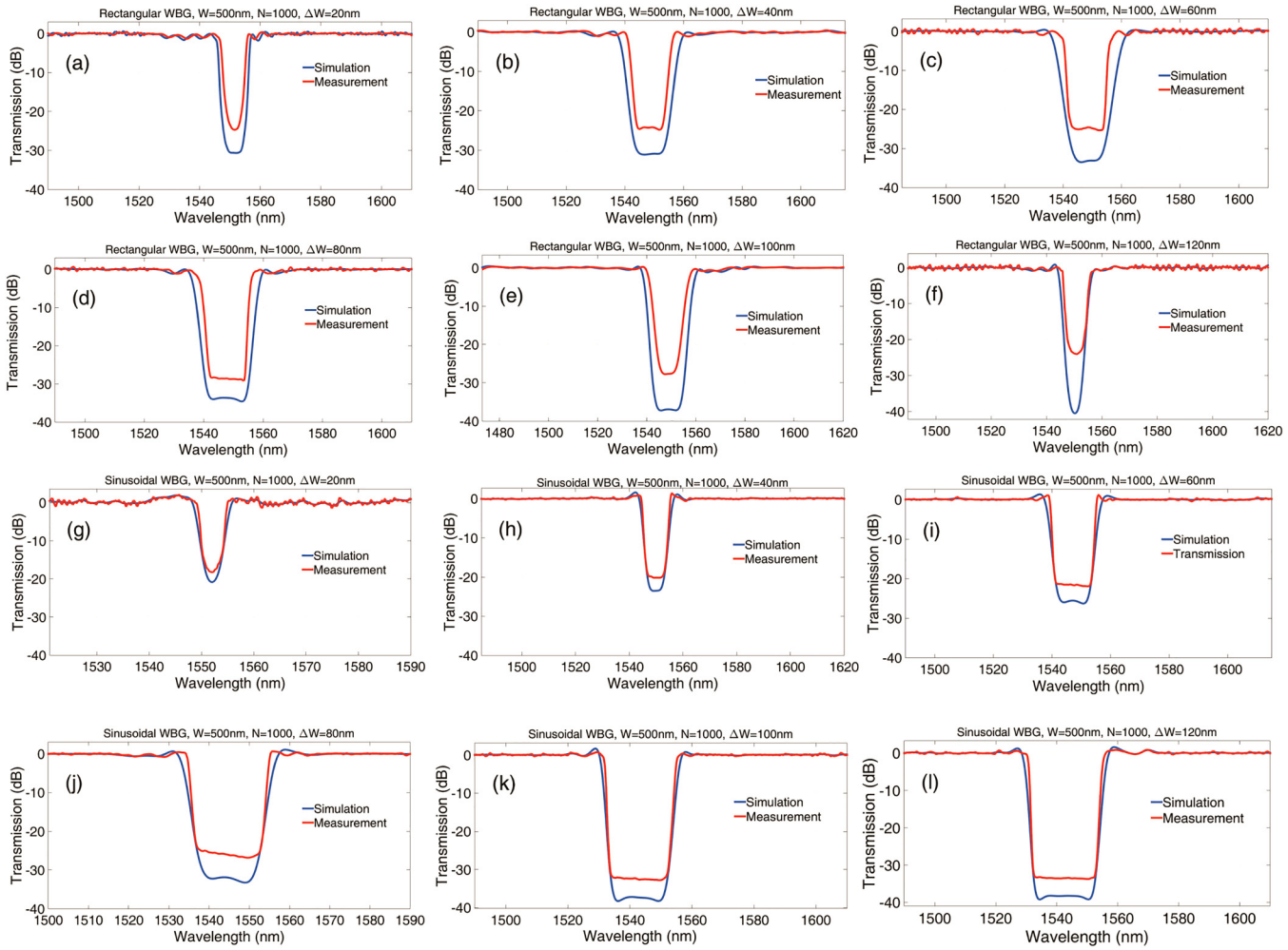

FIG. 8. The transmission spectra of rectangular [(a)–(f)] and sinusoidal [(g)–(l)] WBGs for different values of ΔW in simulation and measurement steps.

a larger grating period, and λ_β increases with increasing Λ. The increment in the Bragg wavelength is about 12.56 nm for both rectangular and sinusoidal WBGs.

Figure 8 shows the simulation and measurement transmission spectra vs wavelength for rectangular and sinusoidal WBGs. As can be observed in this figure, the simulation results for rectangular WBG, Figs. 8(a)–8(f), have more bandwidth than the values obtained from the measurements. However, the measurement values in sinusoidal WBGs, shown in Figs. 8(g)–8(l), are very close to the simulation results, and the FWHM bandwidths for measurements and simulations are almost the same. This indicates that the sinusoidal WBG is less sensitive to the manufacturing process, which is one of its advantages. The comparison of the values of ER and $\Delta\lambda_{FWHM}$ of these structures is fully examined in Figs. 9(g) and 9(h).

Figures 9(a) and 9(b) show the fabricated and designed rectangular WBG with $\Delta W = 20$ nm (in gray and blue). As shown in Fig. 9(a), due to lithography effects, the corrugations of rectangular WBG are significantly smoothed and resemble a sinusoidal WBG. This causes fabricated rectangular WBG to have a narrower bandwidth and ER than the designed rectangular WBG. By contrast, the corrugations of sinusoidal WBG experience minor changes. We used the finite-difference time-domain (FDTD) method to simulate rectangular and sinusoidal WBG spectrums. The measured transmission spectra, ER, and spectral bandwidth profiles vs CW of WBGs with rectangular and sinusoidal sidewalls are plotted in Figs. 9(e)–9(h). As shown in Figs. 9(g) and 9(h), the sinusoidal WBG has a higher bandwidth slope than the rectangular WBG due to a higher fraction of power and larger refractive index variation.

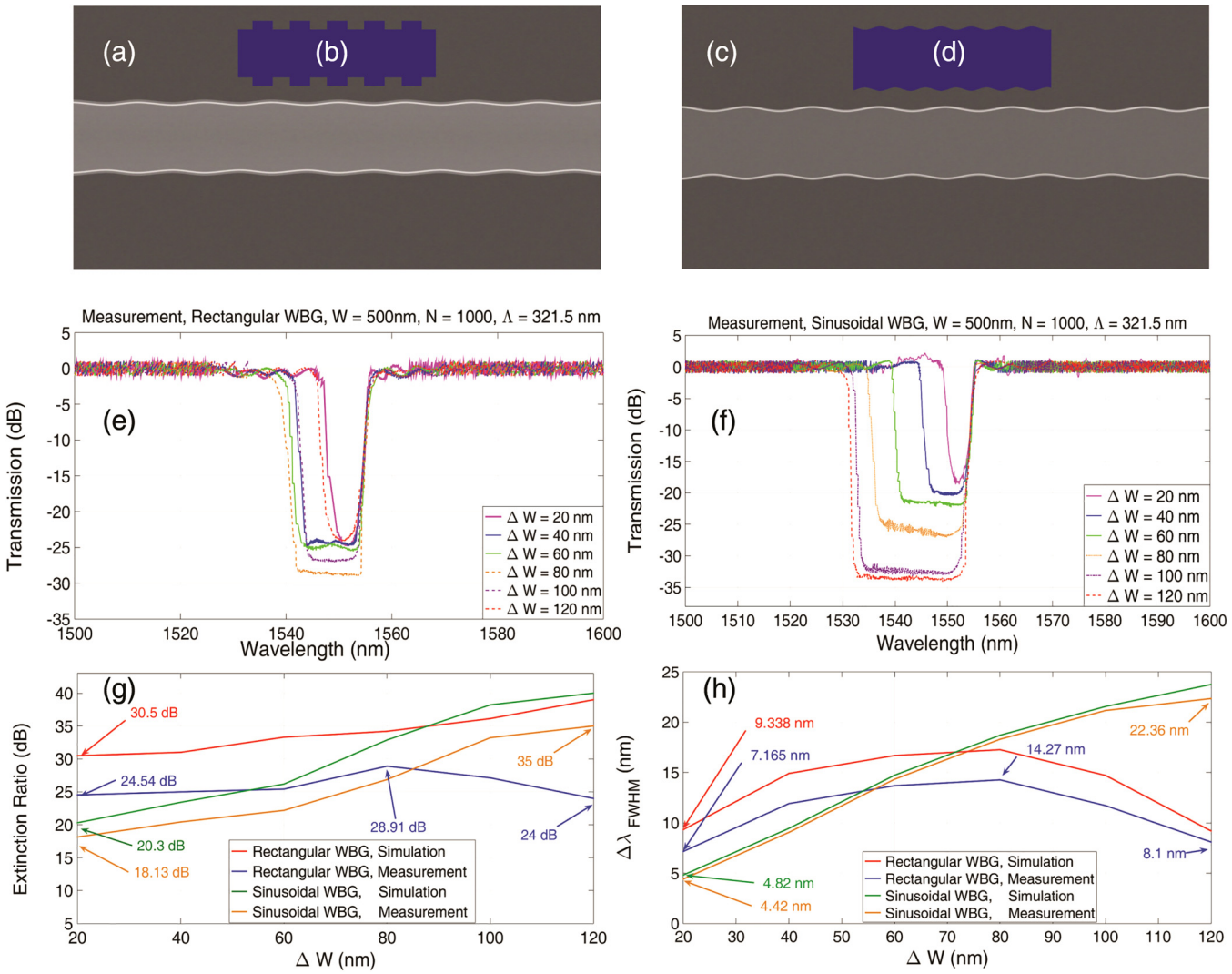

FIG. 9. Fabricated and designed rectangular WBG [(a) and (b)], fabricated and designed sinusoidal WBG [(c) and (d)]. The measured transmission spectra of fabricated WBGs with (e) rectangular and (f) sinusoidal sidewall. (g) Extinction ratio and (h) the full width at half maximum ($\Delta\lambda_{FWHM}$) of each waveguide.

The experimental value of ER saturates to 28.91 dB due to polarization scattering. At the same time, $\Delta\lambda_{FWHM}$ of rectangular WBG reaches its maximum of 14.27 nm at $\Delta W = 80$ nm. For $\Delta W > 80$ nm, the slope of both ER and $\Delta\lambda_{FWHM}$ becomes negative and reaches a minimum of 24 dB and 8.1 nm at $\Delta W = 120$ nm, respectively. In contrast, for $\Delta W > 80$ nm, both ER and $\Delta\lambda_{FWHM}$ of sinusoidal WBG have a positive slope. Based on these characteristics, for designing WDMs with broader bandwidth, sinusoidal WBGs with $\Delta W > 80$ nm are preferable. To obtain a bandwidth below 3 nm, a CW less than 10 nm is required, which is very difficult to fabricate it with small corrugations on the sidewalls.

Figure 10 shows the effect of increasing the waveguide length on the transmission for both the sinusoidal and rectangular waveguides. As the grating number increases from 1000 to 14 000, there is a slight decrease in transmission due to increased propagation loss in the grating waveguide. The propagation loss is within the range of 2.45–4.6 dB/cm, which is very close to that of a straight waveguide without gratings.

When N = 1000, the transmission spectrum resembles an ideal grating response without any ripple. As N increases, the strip (top silicon) thickness varies along the waveguide. It causes fluctuation in the effective index, creating a ripple and blue shift in the transmission spectrum.

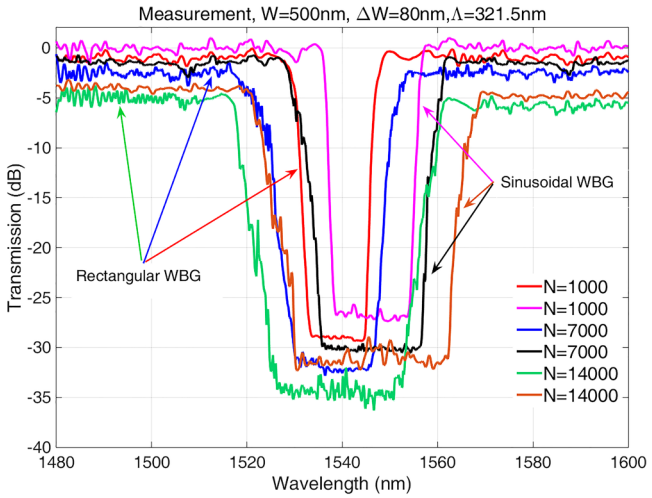

FIG. 10. Measured transmission spectra of sinusoidal and rectangular gratings with fixed (ΔW) = 80 nm for N = 1000, 7000, and 14 000. Showing the effect of bandwidth broadening with increasing N and the variations of wavelength caused by fabrication variations.

VI. CONCLUSION

This paper presented WBGs with rectangular and sinusoidal sidewalls in standard single-mode strip waveguides working at TE polarization. All WBGs and couplers were fabricated using a single-step EBL and etching process. Since this family of devices only requires a single etch, they will find many applications. The results confirm the performance of both the sinusoidal and rectangular gratings as TE polarized band rejection filters used in the telecom C-band and demonstrated ERs as high as 35 dB (28.91 dB) with a rejection bandwidth as narrow as 4.42 nm (6.165 nm) for sinusoidal (rectangular) WBGs. One of the essential characteristics of these waveguides is that we can vary the filter bandwidth and coupling coefficient by altering the corrugation width. This allows to precisely control the filter's quality factor. Since the bandwidth and ER of rectangular WBGs drop for $\Delta W > 80$ nm, sinusoidal WBGs can replace these waveguides in this range. In summary, these integrated Bragg grating devices can pave the way for the fabrication of advanced photonic structures such as tunable laser diodes, silicon photonic biosensors, and tunable transmission filters.

AUTHOR DECLARATIONS

Conflict of Interest

The authors have no conflicts to disclose.

Author Contributions

Hamed Saghaei: Conceptualization (equal); Data curation (equal); Formal analysis (equal); Funding acquisition (equal); Investigation (equal); Methodology (equal); Project administration (equal); Resources (equal); Software (equal); Supervision (equal); Validation (equal); Visualization (equal); Writing – original draft (equal). **Payam Elyasi:** Conceptualization (equal); Data curation (equal); Formal analysis (equal); Funding acquisition (equal); Investigation (equal); Methodology (equal); Project administration (equal); Resources (equal); Software (equal); Supervision (equal); Validation (equal); Visualization (equal); Writing – original draft (equal); Writing – review and editing (equal). **Bhavin J. Shastri:** Conceptualization (equal); Data curation (equal); Formal analysis (equal); Funding acquisition (equal); Investigation (equal); Methodology (equal); Project administration (equal); Resources (equal); Software (equal); Supervision (equal); Validation (equal); Visualization (equal); Writing – original draft (equal); Writing – review and editing (equal).

DATA AVAILABILITY

The data that support the findings of this study are available from the corresponding author upon reasonable request.

REFERENCES

[1]T. E. Murphy, J. T. Hastings, and H. I. Smith, "Fabrication and characterization of narrow-band Bragg-reflection filters in silicon-on-insulator ridge waveguides," J. Lightwave Technol. **19**, 1938 (2001).
[2]M. Burla, L. R. Cortés, M. Li, X. Wang, L. Chrostowski, and J. Azaña, "Integrated waveguide Bragg gratings for microwave photonics signal processing," Opt. Express **21**, 25120–25147 (2013).
[3]R. Loiacono, G. T. Reed, G. Z. Mashanovich, R. Gwilliam, S. J. Henley, Y. Hu, R. Feldesh, and R. Jones, "Laser erasable implanted gratings for integrated silicon photonics," Opt. Express **19**, 10728–10734 (2011).
[4]Q. Fang, J. F. Song, X. Tu, L. Jia, X. Luo, M. Yu, and G. Q. Lo, "Carrier-induced silicon Bragg grating filters with a p-i-n junction," IEEE Photonics Technol. Lett. **25**, 810–812 (2013).
[5]J. T. Hastings, M. H. Lim, J. G. Goodberlet, and H. I. Smith, "Optical waveguides with apodized sidewall gratings via spatial-phase-locked electron-beam lithography," J. Vac. Sci. Technol. B **20**, 2753–2757 (2002).
[6]M. A. Tran, D. Huang, T. Komljenovic, J. Peters, A. Malik, and J. E. Bowers, "Ultra-low-loss silicon waveguides for heterogeneously integrated silicon/III-V photonics," Appl. Sci. **8**, 1139 (2018).
[7]I. Giuntoni, A. Gajda, M. Krause, R. Steingrüber, J. Bruns, and K. Petermann, "Tunable Bragg reflectors on silicon-on-insulator rib waveguides," Opt. Express **17**, 18518–18524 (2009).
[8]W. Bogaerts and S. K. Selvaraja, "Compact single-mode silicon hybrid rib/strip waveguide with adiabatic bends," IEEE Photonics J. **3**, 422–432 (2011).
[9]W. Shi, X. Wang, W. Zhang, L. Chrostowski, and N. Jaeger, "Contradirectional couplers in silicon-on-insulator rib waveguides," Opt. Lett. **36**, 3999–4001 (2011).
[10]C. R. Pollock and M. Lipson, *Integrated Photonics* (Springer, 2003). Vol. 20.
[11]L. Chrostowski and M. Hochberg, *Silicon Photonics Design: From Devices to Systems* (Cambridge University Press, 2015).
[12]X. Wang, W. Shi, R. Vafaei, N. A. Jaeger, and L. Chrostowski, "Uniform and sampled Bragg gratings in SOI strip waveguides with sidewall corrugations," IEEE Photonics Technol. Lett. **23**, 290–292 (2010).
[13]M. Ma, Z. Chen, H. Yun, Y. Wang, X. Wang, N. A. Jaeger, and L. Chrostowski, "Apodized spiral Bragg grating waveguides in silicon-on-insulator," IEEE Photonics Technol. Lett. **30**, 111–114 (2017).
[14]W. Shi, H. Yun, C. Lin, J. Flueckiger, N. A. Jaeger, and L. Chrostowski, "Coupler-apodized Bragg-grating add–drop filter," Opt. Lett. **38**, 3068–3070 (2013).
[15]A. Zhang and L. Hao, "Random phase-shift Bragg grating-based random fiber laser with a half-open cavity," Appl. Opt. **57**, 10017–10021 (2018).

[16]W. Shi, X. Wang, C. Lin, H. Yun, Y. Liu, T. Baehr-Jones, M. Hochberg, N. A. Jaeger, and L. Chrostowski, "Silicon photonic grating-assisted, contra-directional couplers," Opt. Express **21**, 3633–3650 (2013).
[17]B. Naghdi and L. R. Chen, "Silicon photonic contradirectional couplers using subwavelength grating waveguides," Opt. Express **24**, 23429–23438 (2016).
[18]A. Saeki, T. Kozawa, S. Tagawa, and H. B. Cao, "Line edge roughness of a latent image in post-optical lithography," Nanotechnology **17**, 1543 (2006).
[19]Z. Lu, J. Jhoja, J. Klein, X. Wang, A. Liu, J. Flueckiger, J. Pond, and L. Chrostowski, "Performance prediction for silicon photonics integrated circuits with layout-dependent correlated manufacturing variability," Opt. Express **25**, 9712–9733 (2017).
[20]M. A. Baghban, J. Schollhammer, C. Errando-Herranz, K. B. Gylfason, and K. Gallo, "Bragg gratings in thin-film $LiNbO_3$ waveguides," Opt. Express **25**, 32323–32332 (2017).
[21]J. Čtyrokỳ, J. G. Wangüemert-Pérez, P. Kwiecien, I. Richter, J. Litvik, J. H. Schmid, Í. Molina-Fernández, A. Ortega-Moñux, M. Dado, and P. Cheben, "Design of narrowband Bragg spectral filters in subwavelength grating metamaterial waveguides," Opt. Express **26**, 179–194 (2018).
[22]C. Klitis, G. Cantarella, M. J. Strain, and M. Sorel, "High-extinction-ratio TE/TM selective Bragg grating filters on silicon-on-insulator," Opt. Lett. **42**, 3040–3043 (2017).
[23]J. R. Ong, R. Kumar, and S. Mookherjea, "Ultra-high-contrast and tunable-bandwidth filter using cascaded high-order silicon microring filters," IEEE Photonics Technol. Lett. **25**, 1543–1546 (2013).
[24]N. C. Harris, D. Grassani, A. Simbula, M. Pant, M. Galli, T. Baehr-Jones, M. Hochberg, D. Englund, D. Bajoni, and C. Galland, "Integrated source of spectrally filtered correlated photons for large-scale quantum photonic systems," Phys. Rev. X **4**, 041047 (2014).
[25]M. Piekarek, D. Bonneau, S. Miki, T. Yamashita, M. Fujiwara, M. Sasaki, H. Terai, M. G. Tanner, C. M. Natarajan, R. H. Hadfield, J. L. O'Brien, and M. G. Thompson, "High-extinction ratio integrated photonic filters for silicon quantum photonics," Opt. Lett. **42**, 815–818 (2017).
[26]H. Saghaei, P. Elyasi, and R. Karimzadeh, "Design, fabrication, and characterization of Mach–Zehnder interferometers," Photonics Nanostruct.: Fundam. Appl. **37**, 100733 (2019).
[27]M. G. Saber, Z. Xing, D. Patel, E. El-Fiky, N. Abadia, Y. Wang, M. Jacques, M. Morsy-Osman, and D. V. Plant, "A CMOS compatible ultracompact silicon photonic optical add-drop multiplexer with misaligned sidewall Bragg gratings," IEEE Photonics J. **9**, 1–10 (2017).
[28]R. Krishnamoorthy, I. Soubache, and A. Farmani, "Exploring surface plasmon resonance ring resonator structure for high sensitivity and ultra-high-Q optical filter with FDTD method," Opt. Quantum Electron. **54**, 1–13 (2022).
[29]D. Tan, K. Ikeda, R. Saperstein, B. Slutsky, and Y. Fainman, "Chip-scale dispersion engineering using chirped vertical gratings," Opt. Lett. **33**, 3013–3015 (2008).
[30]C. E. Campanella, A. Cuccovillo, C. Campanella, A. Yurt, and V. Passaro, "Fibre Bragg grating based strain sensors: Review of technology and applications," Sensors **18**, 3115 (2018).
[31]A. F. Sayed, F. M. Mustafa, A. A. Khalaf, and M. H. Aly, "An enhanced WDM optical communication system using a cascaded fiber Bragg grating," Opt. Quantum Electron. **52**, 1–21 (2020).
[32]L. Chrostowski, "Silicon photonics for quantum computing with atomic spins," Proc. SPIE **11918**, 119180G (2021).
[33]J. Buus, M.-C. Amann, and D. J. Blumenthal, *Tunable Laser Diodes and Related Optical Sources*, 2nd ed. (John Wiley & Sons, 2005).
[34]Y. Wang, X. Wang, J. Flueckiger, H. Yun, W. Shi, R. Bojko, N. A. Jaeger, and L. Chrostowski, "Focusing sub-wavelength grating couplers with low back reflections for rapid prototyping of silicon photonic circuits," Opt. Express **22**, 20652–20662 (2014).
[35]S. J. McNab, N. Moll, and Y. A. Vlasov, "Ultra-low loss photonic integrated circuit with membrane-type photonic crystal waveguides," Opt. Express **11**, 2927–2939 (2003).
[36]H. Saghaei and V. Van, "Broadband mid-infrared supercontinuum generation in dispersion-engineered silicon-on-insulator waveguide," J. Opt. Soc. Am. B **36**, A193–A202 (2019).
[37]W. Bogaerts, P. Dumon, J. Brouckaert, K. De Vos, D. Taillaert, D. Van Thourhout, and R. Baets, "Ultra-compact optical filters in silicon-on-insulator and their applications," in *2007 4th IEEE International Conference on Group IV Photonics* (IEEE, 2007), pp. 1–3.
[38]L. Chrostowski and K. Iniewski, *High-Speed Photonics Interconnects* (CRC Press, 2017).